

Enhanced adiabatic index for hot neutron-rich matter from microscopic nuclear forces

Yeunhwan Lim^{1,2,3,*} and Jeremy W. Holt^{4,5,†}

¹*Max-Planck-Institut für Kernphysik, Saupfercheckweg 1, 69117 Heidelberg, Germany*

²*Institut für Kernphysik, Technische Universität Darmstadt, 64289 Darmstadt, Germany*

³*ExtreMe Matter Institute EMMI, GSI Helmholtzzentrum für Schwerionenforschung GmbH, 64291 Darmstadt, Germany*

⁴*Cyclotron Institute, Texas A&M University, College Station, TX 77843, USA*

⁵*Department of Physics and Astronomy, Texas A&M University, College Station, TX 77843, USA*

(Dated: September 20, 2019)

We investigate the adiabatic index Γ_{th} of hot and dense nuclear matter from chiral effective field theory and find that the results are systematically larger than from typical mean field models. We start by constructing the finite-temperature equation of state from chiral two- and three-nucleon forces, which we then use to fit a class of extended Skyrme energy density functionals. This allows for modeling the thermal index across the full range of densities and temperatures that may be probed in simulations of core-collapse supernovae and neutron star mergers, including the low-density inhomogeneous mixed phase. For uniform matter we compare the results to analytical expressions for Γ_{th} based on Fermi liquid theory. The correlation between the thermal index and the effective masses at nuclear saturation density is studied systematically through Bayesian modeling of the nuclear equation of state. We then study the behavior of Γ_{th} in both relativistic and non-relativistic mean field models used in the astrophysical simulation community to complement those based on chiral effective field theory constraints from our own study. We derive compact parameterization formulas for Γ_{th} across the range of densities and temperatures encountered in core collapse supernovae and binary neutron star mergers, which we suggest may be useful for the numerical simulation community.

PACS numbers: 21.30.-x, 21.65.Ef

I. INTRODUCTION

Neutron stars are intriguing stellar objects whose structure and dynamics are governed by the properties of matter at extraordinarily high densities up to ten times that of atomic nuclei. Ongoing experimental efforts aim to study the hot and dense matter equation of state (EOS) through medium-energy heavy-ion collisions [1–4], while astronomical observations of neutron star radii, moments of inertia, and tidal deformabilities [5–9] are able to probe the properties of cold compressed matter at around twice nuclear saturation density [10, 11]. In particular, the recent observation of gravitational waves from binary neutron star merger event GW170817 [9, 12] indicates that the tidal deformability of a $1.4 M_{\odot}$ neutron star lies in the range $\Lambda_{1.4} = 190_{-120}^{+390}$. This measurement excludes many stiff equations of state that would give rise to typical neutron stars with radii $R_{1.4} > 13.6$ km [13–17]. Moreover, recent advances in the theoretical description of nuclear forces now enable constraints on the ground state energy and pressure of dense nucleonic matter at and below nuclear saturation density [18–27]. At higher densities theoretical uncertainties grow rapidly [16, 28], and the reliability of microscopic calculations becomes uncertain.

The properties of dense nuclear matter beyond twice saturation density are highly model dependent, and not

even the appropriate degrees of freedom are known. It has been suggested that exotic matter such as hyperons [29–34], kaon or pion condensates [35–41], and strange quarks or deconfined quark matter [42–45] might exist in the inner core of neutron stars. Imprints of this extreme matter might be confirmed through astrophysical observations of pulsar glitches [46–51], X-ray bursts [7, 52–57], neutron star cooling [58–66], neutron star moments of inertia [5, 67–69], and simultaneous measurements of masses and radii, e.g., from the NICER X-ray telescope [70–72]. In order to explore the widest range of high-density parameterizations for the cold dense matter equation of state (including possible phase transitions), theoretical modeling has employed piecewise polytropes [7, 73–75], the spectral representation [76], polynomial expansions in powers of the density or Fermi momentum [15, 77, 78], and speed of sound parameterizations [16, 49, 79].

Dynamical simulations of core-collapse supernovae [80–88] and neutron star mergers [89–98] require also the equation of state at finite temperatures up to 50 – 100 MeV. Such simulations are crucial for interpreting observable electromagnetic, neutrino, and gravitational wave emissions as well as understanding the origin of many heavy elements through r-process nucleosynthesis [97–101]. Presently there exist a number of EOS tabulations derived from Skyrme mean field phenomenology [102–105] and relativistic mean field models [106–111] appropriate for astrophysical simulations. To explore an even wider range of parameterizations, polytropic equations of state have been coupled with an ideal gas ansatz

*Electronic address: ylim@theorie.ikp.physik.tu-darmstadt.de

†Electronic address: holt@physics.tamu.edu

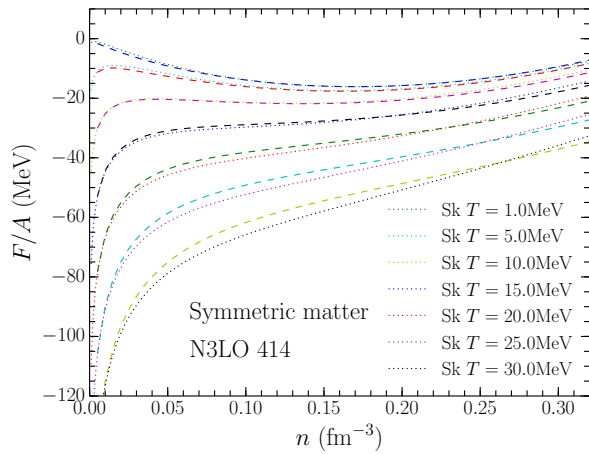


FIG. 1: Free energy per baryon for isospin-symmetric matter as a function of density and temperature computed from the N3LO414 chiral nuclear potential (dashed lines) and the fitted extended Skyrme functional (dotted lines).

for the thermal contribution to the pressure

$$p_{\text{th}} = (\Gamma_{\text{th}} - 1)\varepsilon_{\text{th}}, \quad (1)$$

where ε_{th} is the internal energy density and Γ_{th} is the so-called adiabatic index. The resulting analytical equations of state have numerical advantages over tabulations and allow for a more thorough exploration of the correlations among bulk neutron star properties, features of gravitational wave signals, and properties of the equation of state. In particular, thermal effects have been shown to modify the dominant peak frequency and intensity of the post-merger gravitational wave signal [93, 94] and lead to a delay in the remnant collapse time to a black hole [93, 112].

Previous studies [93, 94, 112] have employed a constant value of the thermal index, and in the present work our aim is to provide a general parameterization for Γ_{th} in terms of the density and temperature based on finite-temperature calculations of the equation of state [113, 114] from microscopic chiral effective field theory (χ EFT). Recent works have also studied the thermal index from microscopic many-body theory [115, 116] and parameterized equations of state [117]. We derive empirical formulas for Γ_{th} as a function of temperature and baryon number density for a proton fraction fixed to that of beta equilibrium matter at $T = 0$ MeV. For this end, we collect EOSs available in the supernova community and build our own EOSs based on χ EFT results for the free energy density. We present fitting functions and covariance matrices that will allow for the generation of realistic behaviors for Γ_{th} as a function of density and temperature within the modeled statistical uncertainties.

The paper is organized as follows. In Section II, we briefly explain the nuclear force models used for constructing the hot and dense matter EOS. In Section III, we present results for Γ_{th} from our current calculations

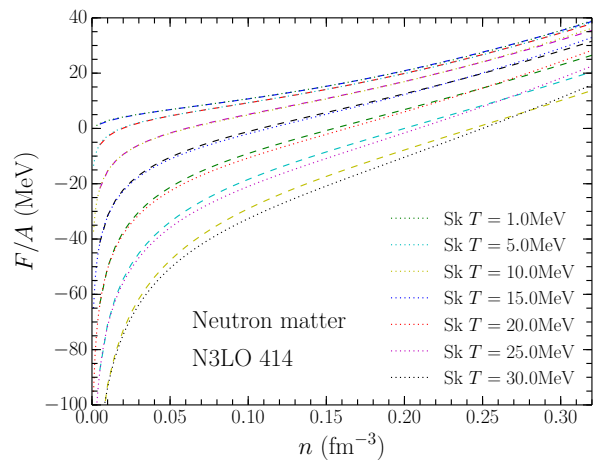


FIG. 2: Free energy per baryon for pure neutron matter as a function of density and temperature computed from the N3LO414 chiral nuclear potential (dashed lines) and the fitted extended Skyrme functional (dotted lines).

based on chiral effective field theory and existing mean field model EOSs. We then derive empirical formulas and covariance matrices for the description of Γ_{th} as a function of density and temperature. In section V, we summarize our results and discuss future directions for modeling the hot and dense matter EOS from realistic nuclear force models.

II. NUCLEAR FORCE MODELS

Nuclear forces derived from chiral effective field theory (χ EFT) are nowadays widely used to study many properties of light and medium-mass nuclei as well as dense uniform matter [118–121]. Recently, chiral nuclear forces have been used to build finite-temperature equations of state based on many-body perturbation theory in the Matsubara imaginary time formalism [113, 114, 122, 123]. However, microscopic calculations break down for the low-density inhomogeneous mixed phase where the spinodal instability is active as well as the high-density phase where chiral effective field theory is no longer applicable. We therefore choose to sample representative calculations of the hot and dense matter equation of state from χ EFT and fit the results to the form of a Skyrme-like potential model. In particular, we employ six different chiral nuclear forces [26]: N2LO450, N2LO500, N3LO414, N3LO450, and N3LO500, corresponding to a next-to-next-to-leading-order (N2LO) chiral potential with momentum-space cutoff $\Lambda_\chi = 450$ MeV, an N2LO chiral potential with momentum-space cutoff $\Lambda_\chi = 500$ MeV, etc. As shown in Figs. 1 and 2, we fit the microscopic results up to $n = 2n_0$ and $T < 30$ MeV. In all cases we verify that the fitted Skyrme potential model satisfies causality and can produce a neutron star with maximum mass $M_{\text{max}} \geq 1.97 M_\odot$. For this reason,

we use the extended Skyrme force model as suggested in Ref. [124], where the two-nucleon interaction has the form,

$$\begin{aligned}
v'_{ij} = & v_{ij} + \frac{t_4}{6}(1 + x_4 P_\sigma) n^{\epsilon_2}(\mathbf{r}) \delta(\mathbf{r}_{ij}) \\
& + \frac{1}{2} t_5 (1 + x_5 P_\sigma) [\mathbf{k}'_{ij} n^{\gamma_1}(\mathbf{r}) \delta(\mathbf{r}_{ij}) + \delta(\mathbf{r}_{ij}) n^{\gamma_1}(\mathbf{r}) \mathbf{k}^2] \\
& + t_6 (1 + x_6 P_\sigma) \mathbf{k}'_{ij} \cdot n^{\gamma_2}(\mathbf{r}) \mathbf{k}_{ij} \delta(\mathbf{r}_{ij}).
\end{aligned} \tag{2}$$

This type of extension gives the energy density of uniform nuclear matter, i.e. without spin-orbit interaction and density gradient contributions, as

$$\begin{aligned}
\mathcal{E} = & \frac{1}{2M_N} (\tau_n + \tau_p) \\
& + (n_n^2 + n_p^2) f_L(n) + 2n_n n_p f_U(n) \\
& + (n_n \tau_n + n_p \tau_p) g_L(n) + (n_n \tau_p + n_p \tau_n) g_U(n),
\end{aligned} \tag{3}$$

where M_N is the nucleon mass, and the number density (n) and kinetic density (τ) are defined as

$$n_t = \frac{1}{\pi^2} \int \frac{k^2 dk}{1 + e^{(\epsilon_t - \mu_t)/T}}, \quad \tau_t = \frac{1}{\pi^2} \int \frac{k^4 dk}{1 + e^{(\epsilon_t - \mu_t)/T}} \tag{4}$$

with μ_t the chemical potential of species $t = p, n$. Here ϵ_t is the single particle energy given by

$$\epsilon_t(k) = \frac{k^2}{2M_t^*} + V_t, \quad \frac{1}{2M_t^*} = \frac{\delta \mathcal{E}}{\delta \tau_t}, \quad V_t = \frac{\delta \mathcal{E}}{\delta n_t}. \tag{5}$$

The functionals $f_{L,U}(n)$ and $g_{L,U}(n)$ are given as

$$\begin{aligned}
f_{L,U}(n) &= \alpha_{L,U} + \eta_{L,U} n^{\epsilon_1} + \lambda_{L,U} n^{\epsilon_2}, \\
g_{L,U}(n) &= \beta_{L,U} + \zeta_{L,U} n^{\gamma_1} + \sigma_{L,U} n^{\gamma_2}.
\end{aligned} \tag{6}$$

Note that the conventional Skyrme force model contains only $\alpha_L, \alpha_U, \beta_L, \beta_U$, and η_L, η_U . However, we use the extended model to obtain a better description of the free energy computed at finite temperature from chiral nuclear potentials.

The effective mass in the extended form is expressed as

$$\frac{1}{2M_N^*} = \frac{1}{2M_N} + g_L(n)n_n + g_U(n)n_p. \tag{7}$$

In contrast to effective masses computed from microscopic nuclear forces, the effective mass from the Skyrme formalism does not depend explicitly on the temperature. In particular, thermal effects are known [125] to strongly suppress the energy dependence of the nucleon single-particle potential, thereby reducing the normally strong enhancement of the effective mass close to the Fermi surface [126, 127]. At high temperatures we therefore expect that the momentum dependence of the nucleon single-particle potential is primarily responsible for the effective mass, which would exhibit a behavior more similar to that given in Eq. (7). However, mean field models may

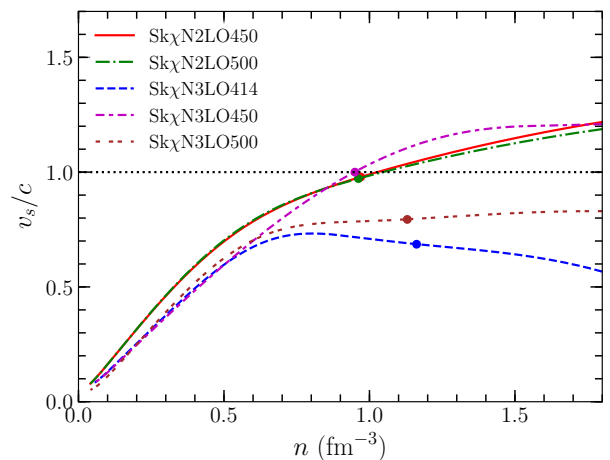


FIG. 3: The speed of sound as a function of density for beta-equilibrated nuclear matter from the five Skyrme energy density functionals constructed in the present work. The dots denote the density of the maximum neutron star mass for each associated equation of state.

not be well suited to reproduce these higher-order temperature effects. When we set the power of the density in the extra effective mass contribution $\gamma_1 = \gamma_2$, we then have ten parameters to be determined for fixed $\epsilon_1 (= 1/3)$, $\epsilon_2 (= 1)$ and $\gamma (= 2/3$ or $1)$. In this work, we use the ten parameters to fit the free energy per baryon from chiral effective field theory calculations at finite temperature as well as zero temperature.

In Fig. 1 and 2 we show the free energy per baryon of symmetric nuclear matter and pure neutron matter as a function of density and temperature from χ EFT (dashed curves) and the corresponding non-relativistic model calculation (dotted curves). We see that as the temperature increases, it becomes more difficult to fit the chiral EFT results to the form of a Skyrme energy density functional, as observed also in Ref. [128]. Note that the Skyrme force model includes only the first-order Hartree-Fock contribution to the free energy. In contrast, the results from chiral effective field theory include second-order contributions plus Hartree-Fock self-energies for the intermediate states as described in Ref. [113].

In Fig. 3 we show the speed of sound in beta stable nuclear matter at $T = 0$ MeV for the five Skyrme interactions fitted in the present work to the hot and dense matter equations of state from chiral effective field theory. We note that some of the models become acausal around $n \simeq 1.0$ fm $^{-3}$, but these densities typically lie beyond the maximal density reached at the center of the maximum mass neutron star. Acausality in non-relativistic models may be remedied in a thermodynamically consistent manner according to the general formalism in Ref. [129] (see also Ref. [123]). In the present work we consider only equations of state that give rise to subluminal speeds of sound at all densities within the neutron stars considered.

In Fig. 4 we plot the nucleon effective mass in both

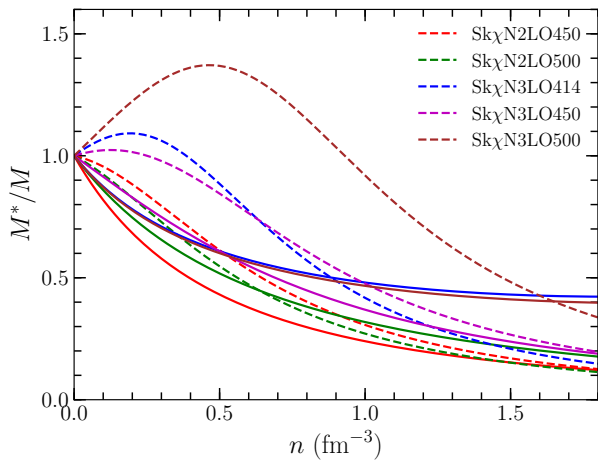


FIG. 4: The neutron effective mass in pure neutron matter (dashed lines) and the nucleon effective mass in symmetric nuclear matter (solid lines) as a function of density for each Skyrme effective interaction constructed in the present work.

symmetric nuclear matter (solid line) and pure neutron matter (dashed lines) for each of the Skyrme effective interactions constructed in the present work. The effective mass is obtained by employing Eq. (7) and fitting the free energy density of nuclear matter computed in chiral effective field theory as described above. We see that at nuclear matter saturation density, the neutron effective mass in pure neutron matter takes on the range of values $0.86 < M^*/M < 1.19$, which is consistent with other phenomenological and microscopic predictions [130, 131]. In symmetric nuclear matter at saturation density, the nucleon effective mass lies in the more narrow range $0.74 < M^*/M < 0.88$, also consistent with previous theoretical modeling [130, 132].

To test the predictions of the different EOS parameterizations, we calculate in Fig. 5 the individual mass-radius relations for cold neutron stars. We see that in all cases the equations of state produce neutron stars satisfying the maximum mass constraint $M_{\max} \gtrsim 1.97 M_{\odot}$ from Refs. [133, 134]. The Skyrme effective interaction fitted to reproduce the equation of state from the N3LO450 chiral nuclear potential is the only one for which the speed of sound becomes superluminal before the maximum neutron star mass is reached. Nevertheless, the reduced maximum mass that is consistent with causality still exceeds $1.97 M_{\odot}$. In our analysis below, we consider only neutron stars for which the speed of sound is subluminal, and therefore we remove the most massive neutron stars produced by the Skyrme N3LO450 interaction. In computing the mass-radius relationships, we have included realistic modeling of the neutron star outer and inner crusts [135]. This occurs when the matter density is below roughly half saturation density and forms nuclear clusters. The composition is therefore ionized heavy nuclei in the inner and outer crust of neutron stars with uniform nuclear matter in the outer core [74, 135–139].

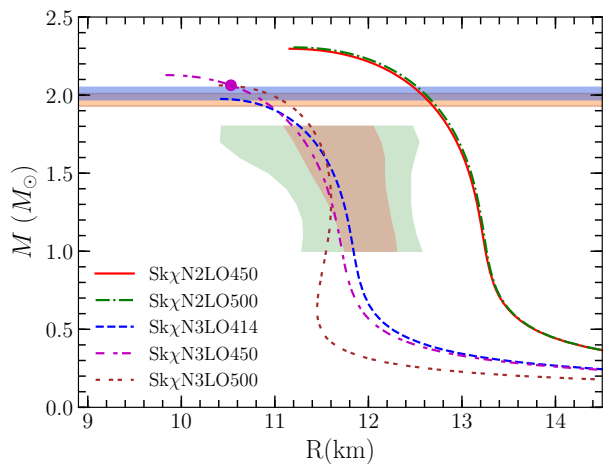


FIG. 5: The neutron star mass-radius relationship for each of the Skyrme effective interactions constructed in the present work. The dot denotes the location at which the Sk χ N3LO450 interaction gives a speed of sound that exceeds the speed of light.

After determining the Skyrme model parameters, we use the liquid drop model technique to construct the hot dense matter EOS. In the liquid drop model, a single heavy nucleus exists in the Wigner-Seitz cell surrounded by a gas of neutrons, protons, electrons, and alpha particles. The free energy density is given by [103, 104],

$$F(n, x, T) = F_{\text{dense}} + F_{\text{dilute}} + F_{\text{surface}} + F_{\text{Coulomb}} + F_{\text{trans}} + F_{\alpha} + F_e + F_{\gamma}, \quad (8)$$

where F_{dense} is the bulk free energy density from the heavy nucleus in the Wigner Seitz cell, F_{dilute} is the free energy density from nucleons outside of the heavy nucleus, F_{surface} is the surface energy density of the heavy nucleus, F_{Coulomb} is the Coulomb energy density between proton-proton, proton-electron, and electron-electron systems, F_{trans} is the translational energy density of the heavy nucleus, F_{α} is the alpha particle free energy density, F_e is the electron (and positron) contribution, and F_{γ} is the photon contribution. We then minimize $F(n, x, T)$ as a function of density, proton fraction and temperature with respect to the dependent variables $(u, n_i, x_i, n_o, x_o, n_{\alpha})$ with the two constraints (i) baryon number conservation and (ii) charge neutrality:

$$\begin{aligned} n &= un_i + (1 - u)[4n_{\alpha} + (1 - n_{\alpha}v_{\alpha})n_o], \\ nx &= un_ix_i + (1 - u)[2n_{\alpha} + (1 - n_{\alpha}v_{\alpha})n_o x_o], \end{aligned} \quad (9)$$

where n_i is the baryon number density of the heavy nucleus, x_i is the proton fraction of the heavy nucleus, n_o is the baryon number density of nucleons outside the heavy nucleus, x_o is the proton fraction of nucleons outside the heavy nucleus, n_{α} is the alpha particle density, and v_{α} is the volume of alpha particle ($v_{\alpha} = 24 \text{ fm}^3$).

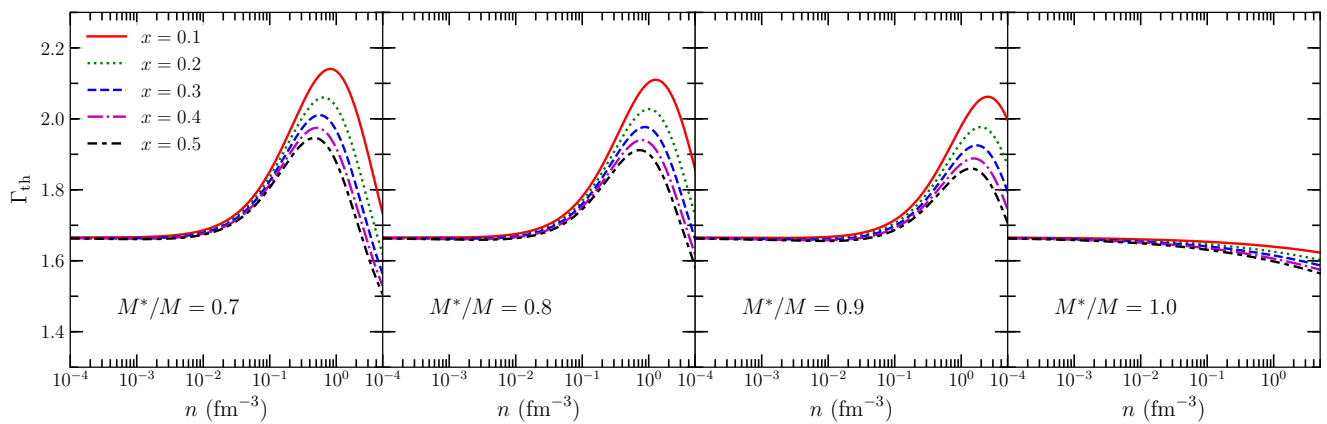


FIG. 6: The thermal index Γ_{th} as a function of density n and proton fraction x calculated in the Fermi liquid theory quasiparticle approximation from Eqs. (11) and (13). The nucleon effective mass as a function of density is assumed to follow the standard Skyrme form, and the value at saturation density is labeled as M^*/M in the different panels.

III. THERMAL INDEX: Γ_{th}

The pressure of nuclear matter can be written as the sum of a zero-temperature contribution and a thermal contribution:

$$p = p_{\text{cold}} + p_{\text{th}}, \quad (10)$$

where all quantities are defined at the same density and proton fraction. Since there are large uncertainties in the nuclear matter equation of state at high densities, it may be useful to first construct the pressure of cold nuclear matter using piecewise polytropes. Theoretical modeling of the thermal contribution p_{th} would then allow for the extension of the equation of state to finite temperature. In the present work we will employ a number of realistic equations of state at non-zero temperature to extract the thermal contribution and develop a useful parameterization with (correlated) uncertainty estimates on the model parameters.

It is natural to formulate the thermal pressure in terms of an adiabatic index Γ_{th} defined as

$$\Gamma_{\text{th}} = \frac{p_{\text{th}}}{\varepsilon_{\text{th}}} + 1, \quad (11)$$

where p_{th} and ε_{th} are the pressure and internal energy density contributions from finite temperature respectively:

$$p_{\text{total}} = p_{\text{th}} + p_{\text{cold}}; \quad \varepsilon_{\text{total}} = \varepsilon_{\text{th}} + \varepsilon_{\text{cold}}. \quad (12)$$

We note that Γ_{th} is a function of the independent variables used for constructing the nuclear EOS. In previous simulations of core-collapse supernovae and neutron star mergers [93, 140], the most widely used values for Γ_{th} are 1.5 or 2.0, which may be obtained by averaging the true adiabatic index from full finite-temperature equations of state over the typical range of temperatures, densities and proton fractions encountered in simulations. Since

Γ_{th} can vary significantly as a function of density and temperature [93], the constant Γ_{th} approximation should be replaced with more realistic modeling.

Fermi liquid theory (FLT) provides a clear conceptual framework based on the quasiparticle approximation to understand the thermal excitations of Fermi systems at low temperatures ($T \ll k_F^2/2M$), and in particular the adiabatic index Γ_{th} . Since the quasiparticle effective mass is directly related to the density of states, it plays a key role in entropy generation and other thermal properties of dense matter. In particular, higher effective masses are associated with a larger density of states and therefore a reduced thermal pressure, leading for instance to faster contraction of a newly-born proto-neutron star following stellar core collapse [141]. From Fermi liquid theory, the thermal contribution to the internal energy density and pressure of nuclear matter composed of protons, neutrons, and electrons is given by [142]

$$\begin{aligned} \varepsilon_{\text{th}} &= \sum_{i=n,p,e} n_i a_i T^2, \\ p_{\text{th}} &= \frac{2}{3} T^2 \sum_{i=n,p,e} a_i n_i \left[1 - \frac{3n_i}{2M_i^*} \frac{\partial M_i^*}{\partial n_i} \right], \end{aligned} \quad (13)$$

where $a = \frac{\pi^2 M^*}{2p_F^2}$ is the level density parameter at the Fermi surface, and the effective mass for relativistic electrons is given as $m_e^* = \sqrt{p_{Fe}^2 + m_e^2}$. Note that for a Fermi gas with fixed composition and temperature-independent effective mass, the FLT approximation does not exhibit a temperature dependence in Γ_{th} .

For orientation, in Fig. 6 we show the parametric dependence of the thermal index Γ_{th} on the effective mass for different values of the proton fraction (x) and the baryon number density (n) using the Fermi liquid theory expressions in Eqs. (11) and (13). For the moment, we assume for simplicity that the nucleon effective mass M^* at the Fermi surface does not vary with the isospin

asymmetry and depends on the baryon number density as in typical Skyrme models:

$$M^* = \frac{M}{1 + \beta n}. \quad (14)$$

Note that in our extended Skyrme parametrization, Eq. (7), the effective mass can have a more complicated density dependence. In Fig. 6 the effective masses are labeled by their values at nuclear matter saturation density n_0 . We see that the behavior of Γ_{th} above about half saturation density is strongly sensitive to the nucleon effective mass. In particular, a lower effective mass naturally gives rise to higher values of Γ_{th} at high density regions.

IV. RESULTS

We now consider two different methods for parameterizing the finite-temperature equation of state based on microscopic many-body calculations. In the first approach we again take a parametrized form for the effective mass, which we then combine with a wide range of cold neutron star equations of state constrained by nuclear theory and experiment [15]. The limitation is that at low density and finite temperature we assume the presence of uniform matter, since constructing an ensemble of nuclei in a gas of unbound protons and neutrons requires additional modeling beyond the level of Fermi liquid theory, e.g., the nucleus volume fraction in the Wigner-Seitz cell approximation. In the second approach we consider full finite-temperature equations of state based on mean field models fitted to results from chiral effective field theory. This allows for a reliable treatment of the inhomogeneous mixed phase at low density and finite temperature. The comparison of the two methods allows us to explore the effects of nuclear clusters on the adiabatic index.

The first approach is based on the Bayesian statistical framework developed in Ref. [15] in which constraints from chiral effective field theory define the prior probability distributions for the parameters \vec{a} and \vec{b} entering in a power series expansion of the zero-temperature equation of state:

$$\begin{aligned} \frac{E}{A}(k_F, x = 0.5) &= 2^{2/3} \frac{3}{5} \frac{k_F^2}{2M} + \frac{k_F^3}{9\pi^2} \sum_{i=0}^3 \frac{a_i}{i!} \beta^i \\ \frac{E}{A}(k_F, x = 0) &= \frac{3}{5} \frac{k_F^2}{2M} + \frac{k_F^3}{9\pi^2} \sum_{i=0}^3 \frac{b_i}{i!} \beta^i, \end{aligned} \quad (15)$$

where E/A is the energy per particle, $\beta \equiv (k_F - k_F^r)/k_F^r$ with k_F^r an arbitrary reference Fermi momentum, and in both expansions we define $k_F = (3\pi^2 n)^{1/3}$. In practice, this is achieved by fitting the equations of state from chiral effective field theory to the form given in Eq. (15) from which we extract the full covariance matrices for the \vec{a} and \vec{b} parameters. Theoretical uncertainties are estimated by varying (i) the order in the chiral expansion,

(ii) the order in the many-body perturbation theory calculation of the equation of state, and (iii) the momentum-space cutoff in the chiral interaction that sets the resolution scale in coordinate space. Experimental data from medium-mass and heavy nuclei (e.g., the saturation energy B and density n_0 of symmetric nuclear matter, the nuclear incompressibility K , and symmetry energy S_2) are then incorporated into Bayesian likelihood functions for the \vec{a} and \vec{b} parameters. This framework allows us to sample a very large set of cold dense matter equations of state for isospin-symmetric nuclear matter and pure neutron matter.

For intermediate values of the proton fraction $x = Z/A$, we expand the free energy per particle F/A in a Taylor series around isospin-symmetric nuclear matter at saturation density:

$$\begin{aligned} \frac{F}{A}(n, x, T) &= \frac{E}{A}(n, x = 0.5, T = 0) + S_2(n)(1 - 2x)^2 \\ &\quad - \frac{T^2}{2n} \left(\frac{\pi}{3}\right)^{2/3} [M_n^* n_n^{1/3} + M_p^* n_p^{1/3}], \end{aligned} \quad (16)$$

where $S_2(n)$ is the density-dependent symmetry energy. In the present work, the Bayesian likelihood function associated with the symmetry energy $S_2(n)$ is constructed from empirical constraints [143] on the symmetry energy at saturation density J together with universal correlations among J , the symmetry energy slope parameter L , and symmetry incompressibility K_{sym} [144]. The proton fraction in beta equilibrium matter can be determined from $S_2(n)$ according to

$$\begin{aligned} \mu_n - \mu_p &= -\frac{\partial f}{\partial x} = \mu_e \\ \implies 4S_2(n)(1 - 2x) &= (3\pi^2 n x)^{1/3}. \end{aligned} \quad (17)$$

The last term in Eq. (16) can be derived in the quasiparticle approximation from Landau Fermi liquid theory at finite temperature.

We note that Eq. (13) does not necessarily describe the thermal contributions to the energy density and pressure at low density, where nuclear matter is clustered. In particular, there is no neutron or proton gas when the density is lower than the neutron drip density $n_{\text{drip}} = 2.4 \times 10^{-4} \text{ fm}^{-3}$. Therefore, the above formula should be reformulated by adding the volume fraction of the heavy nucleus (u) to the Wigner-Seitz cell for the numerical calculation:

$$\varepsilon_{\text{th}} = u \varepsilon_{\text{th}}^{\text{dense}} + (1 - u) \varepsilon_{\text{th}}^{\text{dilute}}. \quad (18)$$

For the pressure, it is not necessary to distinguish $p_{\text{th}}^{\text{dense}}$ and $p_{\text{th}}^{\text{dilute}}$ because $p_{\text{th}}^{\text{dense}} = p_{\text{th}}^{\text{dilute}}$ in the equilibrium state. The volume fraction u should depend on the density and temperature in order to formally obtain the hot dense matter EOS [135].

In the present case the zero-temperature EOS is generated from the liquid drop model [135] to describe nuclear clustering, while at the specific values of temperature $T = 5, 10, 20, 40, 80 \text{ MeV}$ we assume uniform nuclear matter. Note that at finite temperature nuclei can

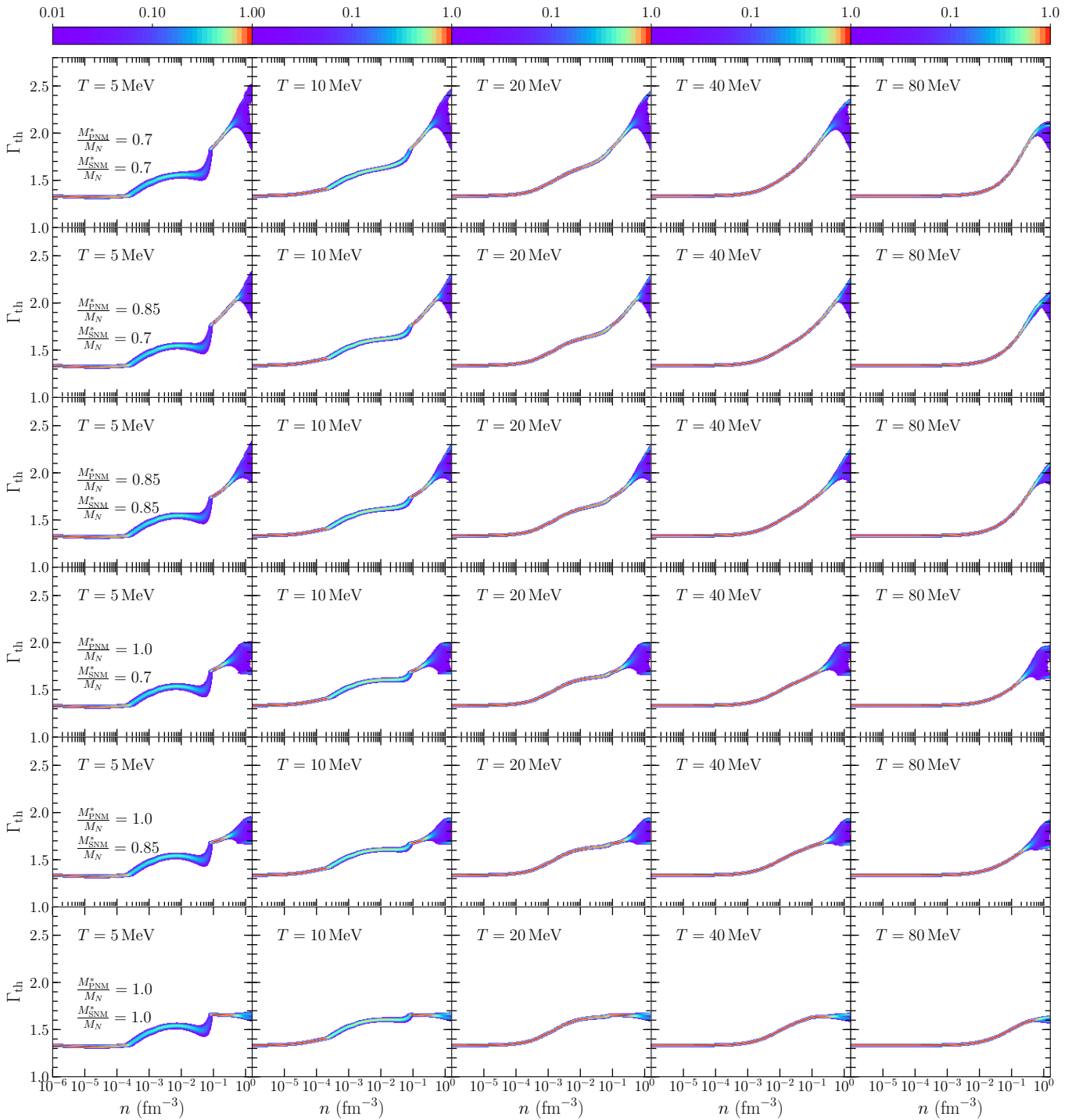


FIG. 7: Contour plots for the adiabatic index Γ_{th} in the Fermi liquid approximation given by Eq. (13) for different values of the nucleon effective mass in symmetric nuclear matter M_{SNM}^*/M_N and pure neutron matter M_{PNM}^*/M_N (labeled by their values at saturation density). The matter composition is obtained by enforcing beta equilibrium on the cold dense matter equation of state sampled within the Bayesian statistical modeling of Ref. [15].

be formed surrounded by unbound neutrons and protons (a situation we will consider at the end of this section). However, if the temperature is greater than the critical temperature of the nuclear liquid-gas phase transition

($T_c \simeq 20$ MeV [114, 122, 145]), all nuclei dissociate and our Fermi liquid theory calculation of the free energy F is well justified. Our Bayesian nuclear modeling does not provide the effective masses in a dense nuclear medium.

In order to include thermal effects, we parameterize Γ_{th} according to different values of the proton and neutron effective masses according to Eqs. (11) and (13). Thus, we take the effective masses of nucleons in symmetric nuclear matter M_{SNM}^* and pure neutron matter M_{PNM}^* at saturation density as parameters within the range of accepted values, while the density dependence follows from Eq. (14).

In Fig. 7 we show the resulting Γ_{th} contour plots as a function of the total baryon number density for labeled values of the nucleon effective masses at nuclear matter saturation density in symmetric nuclear matter M_{SNM}^* and pure neutron matter M_{PNM}^* . Below twice saturation density, Bayesian modeling of the nuclear matter EOS indicates that Γ_{th} converges to a tight range of numerical values for a given set of effective masses. In the present approximation, the adiabatic index is strongly sensitive to the values of the effective masses once the matter composition (as a function of density) is fixed by the underlying cold dense matter equation of state. The error bands shown in Fig. 7 thus reflect uncertainties in the proton fraction coming from the Bayesian modeling of the equation of state. In particular, we see that at low temperatures ($T = 5$ MeV) the contour plots exhibit rather large uncertainties beyond four or five times saturation density when the ratio of the effective mass to bare mass is not 1. This is caused by the fact that some nuclear EOSs from our modeling predict that the ground state energy of pure neutron matter is lower than that of symmetric nuclear matter, so that the Γ_{th} would converge to a finite number:

$$\Gamma_{\text{th}}(n) = 1 + \frac{2}{3} \left[1 - \frac{3n}{2M^*} \frac{\partial M^*}{\partial n} \right] = \frac{5}{3} + \frac{\beta n}{1 + \beta n}. \quad (19)$$

Thus the upper limit of Γ_{th} would become $\Gamma_{\text{th}}(n \rightarrow \infty) = \frac{8}{3}$ which we can see in Fig. 7. In the case of $M_n^*/M = 1$ and $M_p^*/M = 1$ ($\beta = 0$), the value of Γ_{th} becomes $\frac{5}{3}$ as we can see in the bottom of the Fig. 7.

We have seen that the parameterization for proton and neutron effective masses in Eq. (14) does not describe well the results from chiral effective field theory. A more general parameterization based on the extended form of the Skyrme functional may therefore provide a better approximation for the thermal contributions to the pressure and energy density. In our work, we have used $\gamma_1 = \gamma_2 = 1$ in Eq. (6), thus the effective mass is a function of $\beta_{L,U}$ and $\zeta_{L,U}$. The overall density dependence of the effective mass is then described by the mean vector $\mathbf{x} = (\beta_L, \beta_U, \zeta_L, \zeta_U)$ of each coefficient

$$\langle \mathbf{x} \rangle = (-7.61, 71.00, 33.88, -20.39) \quad (20)$$

and its covariance matrix

$$\text{Cov}_{\mathbf{x}} = \begin{pmatrix} 203.45 & -130.00 & 78.95 & 202.92 \\ -130.00 & 329.22 & -36.18 & -202.27 \\ 78.95 & -36.18 & 145.90 & -121.46 \\ 202.92 & -202.27 & -121.46 & 748.91 \end{pmatrix}. \quad (21)$$

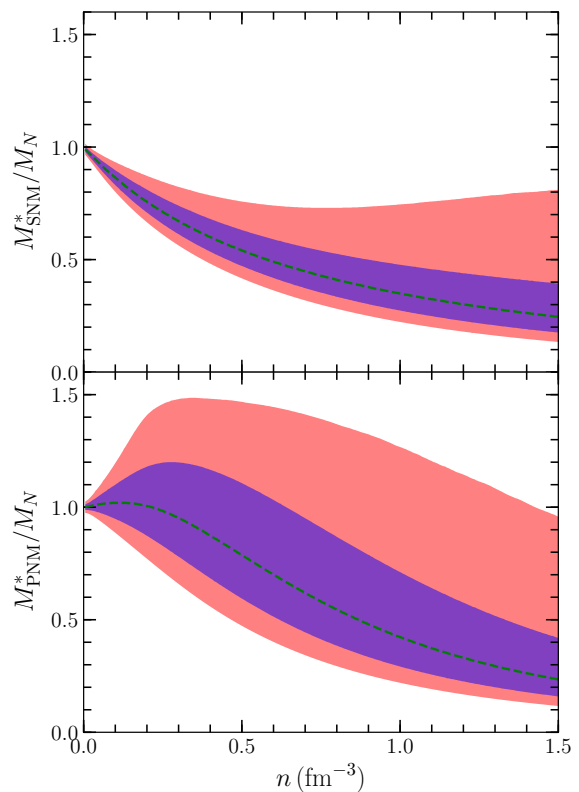


FIG. 8: Uncertainties in the nucleon effective mass in symmetric nuclear matter (top) and pure neutron matter (bottom) obtained from the extended Skyrme force models fitted to χ EFT finite-temperature equations of state.

In Fig. 8 we show the resulting 1σ and 2σ uncertainty bands on the nucleon effective mass in symmetric nuclear matter (top panel) and pure neutron matter (bottom panel) as a function of density in the extended Skyrme mean field models fitted to the hot and dense matter equations of state from chiral effective field theory. The green dashed curves represent the statistical average effective masses among 100,000 effective mass parameter sets. The behavior of effective mass is eventually decreasing as the total baryon number density increases, which guarantees the stabilities of the effective masses.

Next we consider microscopic modeling of thermal effects from finite-temperature quantum many-body theory [113, 114]. In this work, we follow the liquid drop model approach [103] to construct the hot dense matter EOS from Skyrme force models and χ EFT. The basic idea is to find the density of each species in the cell by minimizing the free energy density for a given variable, in general within the three-dimensional space (n, Y_p, T) . Since the nuclear EOS depends on the baryon number density, temperature, and proton fraction, Γ_{th} in general is a function of those variables as well. In the present study we consider the thermal index Γ_{th} for matter in beta-equilibrium, and therefore the proton fraction Y_p is not an independent variable. There is some ambiguity

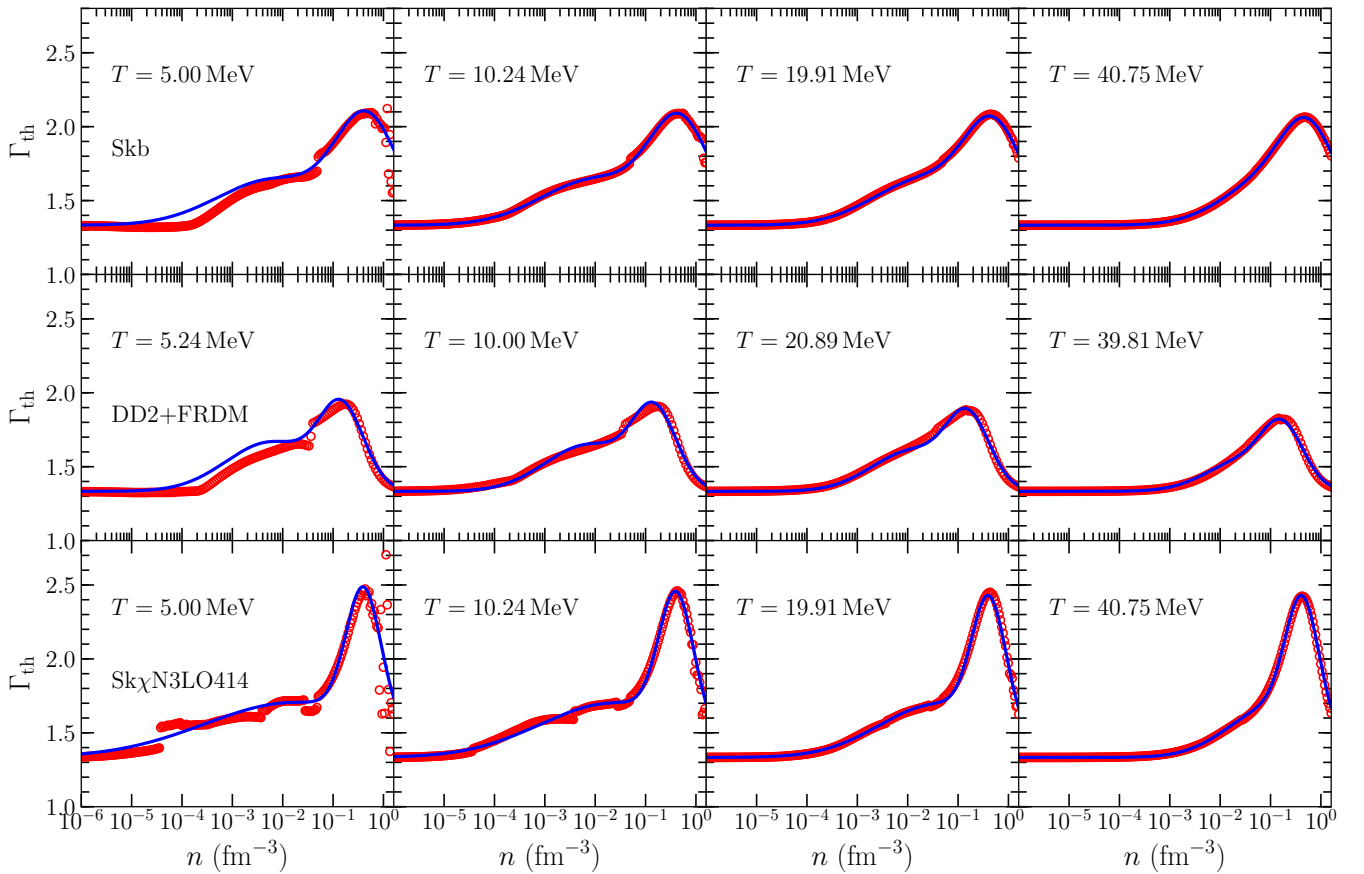


FIG. 9: Density and temperature dependence of Γ_{th} from nuclear equations of state obtained from the mean field models (red circle) Skb, DD2-FRDM, and Sk χ N3LO414 and the fitting function (blue curves) of Eq. (22).

in how we define the proton fraction; whether to use its value at finite temperature or zero temperature. We have computed Γ_{th} in both cases: (i) we use the same proton fraction for both finite temperature and zero temperature and (ii) we determine the proton fraction as a function of temperature for beta equilibrium matter. We have found that there is no significant difference between these two cases. Therefore, we have chosen to use the same proton fraction determined by the zero-temperature beta equilibrium condition also at finite temperature. It is noteworthy that the baryon composition at high temperature becomes isospin-symmetric, since the magnitude of the neutron and proton chemical potentials is much greater than the electron chemical potential.

By considering Γ_{th} from many EOSs, we propose a Γ_{th} fitting function:

$$\Gamma_{\text{th}} = \frac{4}{3} + a \exp[-b(\xi - \xi_a)^2] + c \exp[-d(\xi - \xi_b)^2] \quad (22)$$

where $\xi = \log_{10}(n \text{ fm}^3)$. Note that we have introduced two Gaussian functions that reflect the behavior of Γ_{th} due to two phase transition densities: one for neutron drip and the other for the transition to uniform nuclear matter. The constant $\frac{4}{3}$ corresponds to the low density

($n < 10^{-5} \text{ fm}^{-3}$) region where the dominant contribution to Γ_{th} comes from ultra relativistic electrons. Since Γ_{th} depends on temperature, we assume that the parameters in Eq. (22), $\mathbf{a} = (a, b, c, d, \xi_a, \xi_b)$ are linear functions of the temperature parameter \mathcal{T} :

$$a = a_0 + a_1 \mathcal{T}; \quad \mathcal{T} = \tanh\left(\frac{T}{100 \text{ MeV}}\right). \quad (23)$$

Thus, there are twelve parameters used to fit microscopic calculations of the thermal index as a function of baryon number density and temperature.

In Fig. 9 we show results for Γ_{th} from a representative Skyrme model (Skb), RMF model (DD2+FRDM), and chiral EFT model (Sk χ N3LO414) determined for beta-equilibrium matter. For the relativistic mean field model DD2+FRDM (as well as those considered below), we use the EOS tables generated by Hempel *et al.* [109] to determine the values of Γ_{th} . In Fig. 9 the red circles represent the numerical calculations while the blue curves show the best-fit function of the form given in Eq. (22) fitted to the EOS results for $T \geq 5 \text{ MeV}$. We see that in most cases the chosen fitting function can accurately reproduce the behavior of Γ_{th} for a wide range of densities and temperatures. Overall, the adiabatic index from the micro-

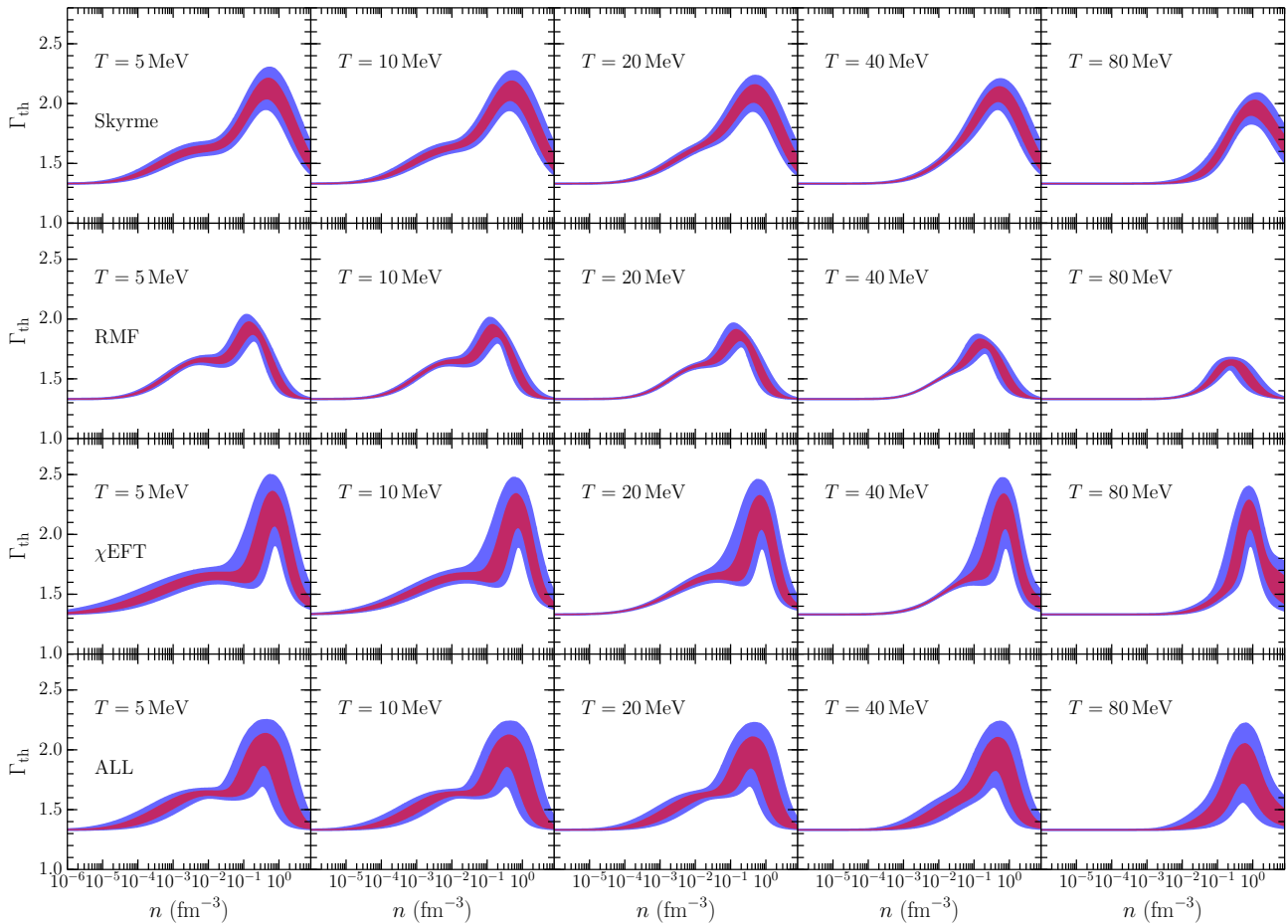


FIG. 10: Confident interval of $\pm 1\sigma$ and $\pm 2\sigma$ obtained from mean vector and covariance matrix for Skyrme, RMF, χ EFT, and all combined models calculations.

scopically constrained $\text{Sk}\chi\text{N3LO414}$ effective interaction exhibits a stronger peak (and a corresponding enhancement of thermal effects in astrophysical simulations) for densities in the range $1 - 2n_0$. Below we will find that this behavior is systematic across a wide range of chiral EFT and mean field models.

For several equations of state we find a discontinuity in Γ_{th} around $n = \frac{1}{2}n_0$ that comes from the phase transition from inhomogeneous nuclear matter to uniform nuclear matter. In these regions the analytical fitting function smooths out the discontinuity. At low temperatures $T < 5$ MeV, nuclear clustering strengthens these discontinuities, leading to less reliable fitting functions. We reiterate that the proton fraction is not constant as a function of the baryon number density since the ground state of nuclear matter is determined by the chemical equilibrium condition $\mu_n = \mu_p + \mu_e$. The effective mass is also not constant but rather has a strong density dependence (see, e.g., Fig. 4 above). In our modeling, the maximum value of Γ_{th} occurs in the density region $n = 0.4 - 0.7 \text{ fm}^{-3}$, which is significantly greater than the value $n = 0.27 \text{ fm}^{-3}$ found in Ref. [142]. We note, however, that in Ref. [142] the density is found in the case

of pure neutron matter. In contrast, we consider beta equilibrium matter which has a finite proton fraction at all densities.

To obtain a representative set of \mathbf{a} parameters, we use various nuclear EOS tables available in the astrophysics simulation communities as well as our own EOS tables [146]. In case of Skyrme force models, we obtain formulas for Γ_{th} using SLy4, SkI4, SkM*, Ska, and Skb. For RMF models we include DD2, FSG, IU-FSU, SFHo, SFHx, TM1, and TMA. Finally, for χ EFT we use results from Skyrme interactions fitted to the finite-temperature equations of state from the N2LO450, N2LO500, N3LO414, N3LO450, and N3LO500 chiral potentials. We estimate theoretical uncertainties in \mathbf{a} from the nuclear force models by constructing the covariance matrix with elements

$$\mathbf{M}_{ij} = \langle (x_i - \langle x_i \rangle)(x_j - \langle x_j \rangle) \rangle. \quad (24)$$

The covariance matrices for the three different classes of interactions as well as the combination of all models are given by

$$\mathbf{v}_{\text{Sk}} = \begin{bmatrix} a_0 & a_1 & b_0 & b_1 & c_0 & c_1 & d_0 & d_1 & \xi_{a_0} & \xi_{a_1} & \xi_{b_0} & \xi_{b_1} \end{bmatrix} \quad (25a)$$

$$\mathbf{M}_{\text{Sk}} = \begin{bmatrix} a_0 & a_1 & b_0 & b_1 & c_0 & c_1 & d_0 & d_1 & \xi_{a_0} & \xi_{a_1} & \xi_{b_0} & \xi_{b_1} \\ a_0 & 1.01e-3 & -2.50e-3 & -3.66e-4 & 1.96e-3 & -1.67e-3 & 3.47e-3 & 9.81e-4 & 2.65e-3 & 3.22e-3 & -1.37e-2 & -4.63e-4 & 1.85e-3 \\ a_1 & -2.50e-3 & 9.70e-3 & 1.78e-4 & -3.06e-3 & 2.04e-3 & -1.22e-2 & -1.06e-3 & -3.73e-3 & -2.12e-3 & 2.60e-2 & -3.58e-3 & -1.11e-2 \\ b_0 & -3.66e-4 & 1.78e-4 & 1.14e-3 & -4.36e-3 & 4.20e-3 & -2.32e-3 & -2.47e-3 & -6.19e-3 & -9.62e-3 & 2.69e-2 & 4.56e-3 & 2.43e-3 \\ b_1 & 1.96e-3 & -3.06e-3 & -4.36e-3 & 1.92e-2 & -1.76e-2 & 2.11e-2 & 9.95e-3 & 2.65e-2 & 3.77e-2 & -1.26e-1 & -1.31e-2 & 2.79e-3 \\ c_0 & -1.67e-3 & 2.04e-3 & 4.20e-3 & -1.76e-2 & 4.11e-3 & -3.99e-3 & -2.32e-3 & -6.11e-3 & -9.02e-3 & 2.83e-2 & 3.56e-3 & 3.82e-4 \\ c_1 & 3.47e-3 & -1.22e-2 & -2.32e-3 & 2.11e-2 & -3.99e-3 & 1.65e-2 & 1.78e-3 & 6.54e-3 & 5.91e-3 & -4.23e-2 & 3.12e-3 & 1.40e-2 \\ d_0 & 9.81e-4 & -1.06e-3 & -2.47e-3 & 9.95e-3 & -2.32e-3 & 1.78e-3 & 6.04e-3 & 1.42e-2 & 2.07e-2 & -6.19e-2 & -8.93e-3 & -3.68e-3 \\ d_1 & 2.65e-3 & -3.73e-3 & -6.19e-3 & 2.65e-2 & -6.11e-3 & 6.54e-3 & 1.42e-2 & 3.68e-2 & 5.30e-2 & -1.71e-1 & -1.98e-2 & -2.63e-5 \\ \xi_{a_0} & 3.22e-3 & -2.12e-3 & -9.62e-3 & 3.77e-2 & -9.02e-3 & 5.91e-3 & 2.07e-2 & 5.30e-2 & 2.05e-2 & -5.89e-2 & -9.31e-3 & -4.06e-3 \\ \xi_{a_1} & -1.37e-2 & 2.60e-2 & 2.69e-2 & -1.26e-1 & 2.83e-2 & -4.23e-2 & -6.19e-2 & -1.71e-1 & -5.89e-2 & -1.71e-1 & 1.69e-2 & -1.41e-2 \\ \xi_{b_0} & -4.63e-4 & -3.58e-3 & 4.56e-3 & -1.31e-2 & 3.56e-3 & 3.12e-3 & -8.93e-3 & -1.98e-2 & -9.31e-3 & 1.69e-2 & 6.52e-3 & 7.79e-3 \\ \xi_{b_1} & 1.85e-3 & -1.11e-2 & 2.43e-3 & 2.79e-3 & 3.82e-4 & 1.40e-2 & -3.68e-3 & -2.63e-5 & -4.06e-3 & -1.41e-2 & 7.79e-3 & 1.65e-2 \end{bmatrix} \quad (25b)$$

$$\mathbf{v}_{\text{RMF}} = \begin{bmatrix} a_0 & a_1 & b_0 & b_1 & c_0 & c_1 & d_0 & d_1 & \xi_{a_0} & \xi_{a_1} & \xi_{b_0} & \xi_{b_1} \end{bmatrix} \quad (26a)$$

$$\mathbf{M}_{\text{RMF}} = \begin{bmatrix} a_0 & a_1 & b_0 & b_1 & c_0 & c_1 & d_0 & d_1 & \xi_{a_0} & \xi_{a_1} & \xi_{b_0} & \xi_{b_1} \\ a_0 & 4.90e-4 & -5.97e-4 & -2.30e-4 & 8.91e-4 & 2.65e-4 & 3.39e-5 & 6.48e-3 & 5.00e-3 & 2.00e-3 & -4.03e-3 & 1.10e-4 & -9.73e-4 \\ a_1 & -5.97e-4 & 7.95e-4 & 1.42e-4 & -8.12e-4 & -6.03e-4 & 3.63e-4 & -9.69e-3 & -6.33e-3 & -2.40e-3 & 5.33e-3 & 4.55e-4 & 1.82e-3 \\ b_0 & -2.30e-4 & 1.42e-4 & 8.09e-4 & -1.87e-3 & 1.03e-3 & -1.83e-3 & 2.18e-3 & -4.21e-3 & -2.06e-3 & 2.05e-3 & -2.54e-3 & -1.70e-3 \\ b_1 & 8.91e-4 & -8.12e-4 & -1.87e-3 & 6.99e-3 & -1.37e-3 & 3.10e-3 & 6.88e-3 & 2.38e-2 & 6.92e-3 & -1.24e-2 & 1.47e-3 & 3.35e-3 \\ c_0 & 2.65e-4 & -6.03e-4 & 1.03e-3 & -1.37e-3 & 1.67e-3 & -1.99e-3 & 1.35e-2 & 1.39e-3 & 9.12e-4 & -3.80e-3 & -1.98e-3 & -3.48e-3 \\ c_1 & 3.39e-5 & 3.63e-4 & -1.83e-3 & 3.10e-3 & -1.99e-3 & 2.77e-3 & -1.25e-2 & 2.85e-4 & 4.49e-4 & 2.22e-3 & 3.55e-3 & 3.83e-3 \\ d_0 & 6.48e-3 & -9.69e-3 & 2.18e-3 & 6.88e-3 & 1.35e-2 & -1.25e-2 & 3.05e-1 & 1.05e-1 & 5.15e-2 & -1.26e-1 & -1.88e-2 & -6.61e-2 \\ d_1 & 5.00e-3 & -6.33e-3 & -4.21e-3 & 2.38e-2 & 1.39e-3 & 2.85e-4 & 1.05e-1 & 1.65e-1 & 3.77e-2 & -9.13e-2 & -2.32e-2 & -1.22e-2 \\ \xi_{a_0} & 2.00e-3 & -2.40e-3 & -2.06e-3 & 6.92e-3 & 9.12e-4 & 4.49e-4 & 5.15e-2 & 3.77e-2 & 8.30e-3 & -1.60e-2 & 1.52e-3 & -3.98e-3 \\ \xi_{a_1} & -4.03e-3 & 5.33e-3 & 2.05e-3 & -1.24e-2 & -3.80e-3 & 2.22e-3 & -1.26e-1 & -9.13e-2 & -1.60e-2 & 3.62e-2 & 4.01e-3 & 1.13e-2 \\ \xi_{b_0} & 1.10e-4 & 4.55e-4 & -2.54e-3 & 1.47e-3 & -1.98e-3 & 3.55e-3 & -1.88e-2 & -2.32e-2 & 1.52e-3 & 4.01e-3 & 9.70e-3 & 2.90e-3 \\ \xi_{b_1} & -9.73e-4 & 1.82e-3 & -1.70e-3 & 3.35e-3 & -3.48e-3 & 3.83e-3 & -6.61e-2 & -1.22e-2 & -3.98e-3 & 1.13e-2 & 2.90e-3 & 9.14e-3 \end{bmatrix} \quad (26b)$$

$$\mathbf{v}_{\text{EFT}} = \begin{bmatrix} a_0 & a_1 & b_0 & b_1 & c_0 & c_1 & d_0 & d_1 & \xi_{a_0} & \xi_{a_1} & \xi_{b_0} & \xi_{b_1} \end{bmatrix} \quad (27a)$$

$$\mathbf{M}_{\chi\text{EFT}} = \begin{bmatrix} a_0 & a_1 & b_0 & b_1 & c_0 & c_1 & d_0 & d_1 & \xi_{a_0} & \xi_{a_1} & \xi_{b_0} & \xi_{b_1} \\ a_0 & 1.58e-3 & -4.21e-3 & -2.10e-3 & 1.28e-2 & 5.97e-4 & 4.18e-3 & -8.42e-3 & -1.29e-1 & -7.71e-4 & -8.01e-3 & -1.66e-3 & 8.11e-4 \\ a_1 & -4.21e-3 & 2.16e-2 & 5.73e-3 & -3.68e-2 & 6.80e-3 & -2.50e-2 & -1.09e-1 & 2.61e-1 & 2.57e-3 & 5.23e-2 & -1.46e-3 & -1.66e-3 \\ b_0 & -2.10e-3 & 5.73e-3 & 2.93e-3 & -1.68e-2 & -1.42e-3 & -6.07e-3 & 7.11e-3 & 1.63e-1 & 3.59e-4 & 1.09e-2 & 1.71e-3 & -7.92e-4 \\ b_1 & 1.28e-2 & -3.68e-2 & -1.68e-2 & 1.12e-1 & -7.40e-4 & 3.79e-2 & -3.84e-3 & -1.10e+0 & -3.70e-3 & -1.00e-1 & -2.28e-2 & 1.02e-2 \\ c_0 & 5.97e-4 & 6.80e-3 & -1.42e-3 & -7.40e-4 & 1.27e-2 & -8.39e-3 & -9.72e-2 & -4.60e-2 & 1.97e-3 & 3.12e-2 & -2.27e-4 & -2.48e-3 \\ c_1 & 4.18e-3 & -2.50e-2 & -6.07e-3 & 3.79e-2 & -8.39e-3 & 3.04e-2 & 1.61e-1 & -2.28e-1 & -6.66e-4 & -6.57e-2 & 3.03e-3 & 1.40e-3 \\ d_0 & -8.42e-3 & -1.09e-1 & 7.11e-3 & -3.84e-3 & -9.72e-2 & 1.61e-1 & 1.95e+0 & 1.65e+0 & 2.00e-2 & -4.50e-1 & 4.97e-2 & -7.51e-3 \\ d_1 & -1.29e-1 & 2.61e-1 & 1.63e-1 & -1.10e+0 & -4.60e-2 & -2.28e-1 & 1.65e+0 & 1.22e+1 & 5.04e-2 & 6.67e-1 & 2.92e-1 & -1.22e-1 \\ \xi_{a_0} & -7.71e-4 & 2.57e-3 & 3.59e-4 & -3.70e-3 & 1.97e-3 & -6.66e-4 & 2.00e-2 & 5.04e-2 & 5.01e-3 & -6.50e-3 & -2.20e-3 & 1.11e-4 \\ \xi_{a_1} & -8.01e-3 & 5.23e-2 & 1.09e-2 & -1.00e-1 & 3.12e-2 & -6.57e-2 & -4.50e-1 & 6.67e-1 & -6.50e-3 & 2.25e-1 & 2.56e-2 & -1.47e-2 \\ \xi_{b_0} & -1.66e-3 & -1.46e-3 & 1.71e-3 & -2.28e-2 & -2.27e-4 & 3.03e-3 & 4.97e-2 & 2.92e-1 & -2.20e-3 & 2.56e-2 & 1.91e-2 & -6.24e-3 \\ \xi_{b_1} & 8.11e-4 & -1.66e-3 & -7.92e-4 & 1.02e-2 & -2.48e-3 & 1.40e-3 & -7.51e-3 & -1.22e-1 & 1.11e-4 & -1.47e-2 & -6.24e-3 & 2.88e-3 \end{bmatrix} \quad (27b)$$

$$\mathbf{v}_{\text{All}} = \begin{bmatrix} a_0 & a_1 & b_0 & b_1 & c_0 & c_1 & d_0 & d_1 & \xi_{a_0} & \xi_{a_1} & \xi_{b_0} & \xi_{b_1} \end{bmatrix} \quad (28a)$$

$$\mathbf{M}_{\text{All}} = \begin{bmatrix} a_0 & a_1 & b_0 & b_1 & c_0 & c_1 & d_0 & d_1 & \xi_{a_0} & \xi_{a_1} & \xi_{b_0} & \xi_{b_1} \\ a_0 & 5.03e-4 & -1.82e-3 & -6.10e-5 & 7.91e-4 & -5.95e-4 & 1.40e-3 & 1.04e-3 & -2.89e-3 & 8.03e-4 & -6.68e-3 & -1.25e-3 & -8.61e-5 \\ a_1 & -1.82e-3 & 1.22e-2 & -7.84e-4 & -2.43e-3 & 6.52e-3 & -4.30e-3 & -4.43e-3 & 1.81e-2 & 2.11e-3 & 3.67e-2 & 1.10e-2 & -1.99e-3 \\ b_0 & -6.10e-5 & -7.84e-4 & 1.50e-3 & -1.43e-3 & -3.41e-3 & -6.22e-3 & -7.04e-3 & -1.77e-2 & -8.82e-3 & -2.66e-3 & -9.37e-3 & 3.82e-3 \\ b_1 & 7.91e-4 & -2.43e-3 & -1.43e-3 & 7.52e-3 & -4.28e-3 & 1.58e-2 & 1.46e-2 & -1.02e-2 & 1.27e-2 & -5.82e-2 & -6.23e-3 & -2.68e-3 \\ c_0 & -5.95e-4 & 6.52e-3 & -3.41e-3 & -4.28e-3 & 5.74e-3 & -1.13e-3 & -2.29e-3 & 7.03e-3 & 1.94e-3 & 2.23e-2 & 7.58e-3 & -1.81e-3 \\ c_1 & 1.40e-3 & -4.30e-3 & -6.22e-3 & 1.58e-2 & -1.13e-3 & 1.20e-2 & 1.42e-2 & 1.38e-2 & 9.24e-3 & -2.43e-2 & 4.88e-3 & -2.86e-3 \\ d_0 & 1.04e-3 & -4.43e-3 & -7.04e-3 & 1.46e-2 & -2.29e-3 & 1.42e-2 & 1.41e-1 & 1.99e-1 & 7.50e-2 & -1.87e-1 & 3.04e-2 & -3.65e-2 \\ d_1 & -2.89e-3 & 1.81e-2 & -1.77e-2 & -1.02e-2 & 7.03e-3 & 1.38e-2 & 1.99e-1 & 7.44e-1 & 1.66e-1 & 6.25e-2 & 1.76e-1 & -9.02e-2 \\ \xi_{a_0} & 8.03e-4 & 2.11e-3 & -8.82e-3 & 1.27e-2 & 1.94e-3 & 9.24e-3 & 7.50e-2 & 1.66e-1 & 1.53e-2 & -1.58e-2 & 7.78e-3 & -6.43e-3 \\ \xi_{a_1} & -6.68e-3 & 3.67e-2 & -2.66e-3 & -5.82e-2 & 2.23e-2 & -2.43e-2 & -1.87e-1 & 6.25e-2 & -1.58e-2 & 1.58e-1 & 3.34e-2 & 1.47e-3 \\ \xi_{b_0} & -1.25e-3 & 1.10e-2 & -9.37e-3 & -6.23e-3 & 7.58e-3 & 4.88e-3 & 3.04e-2 & 1.76e-1 & 7.78e-3 & 3.34e-2 & 2.5e-2 & -4.67e-3 \\ \xi_{b_1} & -8.61e-5 & -1.99e-3 & 3.82e-3 & -2.68e-3 & -1.81e-3 & -2.86e-3 & -3.65e-2 & -9.02e-2 & -6.43e-3 & 1.47e-3 & -4.67e-3 & 4.69e-3 \end{bmatrix} \quad (28b)$$

These numerical results can be used to generate new Γ_{th} parameters within uncertainties originated from nuclear

model differences.

In Fig. 10 we show the 1σ and 2σ uncertainty bands obtained from the mean values and covariance matrices in Eqs. (25)–(28). We see that as the temperature increases, the first inflection point disappears and the maximum value of Γ_{th} decreases in all cases. In contrast to the results shown in Fig. 7, none of the mean field models considered in this section gives rise to a supersoft symmetry energy that would result in pure neutron matter as a ground state at some large density. Therefore, the value of the adiabatic index never reaches the limiting case $\Gamma_{\text{th}} \rightarrow \frac{8}{3}$ as indicated in Eq. (19) where the low temperature approximation is valid. Compared with Skyrme and χ EFT interactions, the confidence band for RMF models is rather small. This may indicate that the range of effective masses in the RMF considered in this work is smaller than from Skyrme and χ EFT interactions.

V. SUMMARY

We have investigated the thermal index Γ_{th} of hot and dense nuclear matter from microscopic many-body calculations based on chiral two- and three-body interactions as well as from Skyrme and relativistic mean field models commonly used in the literature. We find that Γ_{th} depends strongly on the density, temperature, and proton fraction. In the Fermi liquid approximation, Γ_{th} depends essentially on the proton and neutron effective masses at and above nuclear saturation density. However, the simple formulas for the thermal energy density and pressure are valid only in the low-temperature range (low compared with the Fermi temperature). The nucleon effective mass itself is expected to depend sensitively on the temperature [125], and as a result simple Skyrme force models cannot reproduce perfectly the finite-temperature results from chiral effective field theory.

We have parameterized Γ_{th} in terms of the nucleon effective masses in symmetric nuclear matter and pure neutron matter by subtracting the internal energy density and pressure of the cold nuclear matter EOS constructed in the liquid drop model technique from the values in

uniform nuclear matter at finite temperature. From this method, where the cold dense matter equation of state is sampled from a Bayesian posterior probability distribution constrained by nuclear theory and experiment, we have obtained statistical uncertainties on the value of Γ_{th} . As predicted from the Fermi liquid theory description of nuclear matter, Γ_{th} sensitively depends on proton and neutron effective masses.

Finally, we extracted Γ_{th} from realistic hot and dense matter equations of state based on several Skyrme force models, relativistic mean field models, and results from χ EFT that include an accurate treatment of the inhomogeneous mixed phase at low density and finite temperature. We considered the case of matter in beta equilibrium, from which we determined the proton fraction as a function of density. The mean field models constrained by microscopic chiral effective field theory were found to exhibit a consistently larger adiabatic index compared to traditional Skyrme force models and especially relativistic mean field models. From these results we have suggested a simple but accurate phenomenological formula for Γ_{th} written as a function of density and temperature. By combining the different models, we obtained mean values for the Γ_{th} parameters and their corresponding covariance matrices. This parametrization can be used to supplement a wide range of cold equations of state for use in core-collapse supernova or neutron star merger simulations.

Acknowledgments

We thank A. Bauswein for discussion. Work supported by the National Science Foundation under grant No. PHY1652199. Portions of this research were conducted with the advanced computing resources provided by Texas A&M High Performance Research Computing. Y. Lim was also supported by the Max Planck Society and the Deutsche Forschungsgemeinschaft (DFG, German Research Foundation) – Projektnummer 279384907 – SFB 1245.

-
- [1] P. Danielewicz, R. Lacey, and W. G. Lynch, *Science* **298**, 1592 (2002).
 - [2] M. Tsang, T. Liu, L. Shi, P. Danielewicz, C. Gelbke, X. Liu, W. Lynch, W. Tan, G. Verde, A. Wagner, *et al.*, *Phys. Rev. Lett.* **92**, 062701 (2004).
 - [3] D. V. Shetty, S. J. Yennello, and G. A. Souliotis, *Phys. Rev. C* **75**, 034602 (2007).
 - [4] L. Qin *et al.*, *Phys. Rev. Lett.* **108**, 172701 (2012).
 - [5] J. M. Lattimer and B. F. Schutz, *Astrophys. J.* **629**, 979 (2005).
 - [6] A. Steiner, M. Prakash, J. Lattimer, and P. Ellis, *Phys. Rept.* **411**, 325 (2005).
 - [7] A. W. Steiner, J. M. Lattimer, and E. F. Brown, *Astrophys. J.* **722**, 33 (2010).
 - [8] J. M. Lattimer and A. W. Steiner, *Eur. Phys. J.* **A50**, 40 (2014).
 - [9] B. P. Abbott *et al.* (The LIGO Scientific Collaboration and the Virgo Collaboration), *Phys. Rev. Lett.* **121**, 161101 (2018).
 - [10] J. M. Lattimer and M. Prakash, *Astrophys. J.* **550**, 426 (2001).
 - [11] J. W. Holt and Y. Lim, *AIP Conf. Proc.* **2127**, 020019 (2019).
 - [12] B. P. Abbott *et al.* (LIGO Scientific Collaboration and Virgo Collaboration), *Phys. Rev. Lett.* **119**, 161101 (2017).

- [13] F. J. Fattoyev, J. Piekarewicz, and C. J. Horowitz, *Phys. Rev. Lett.* **120**, 172702 (2018).
- [14] E. R. Most, L. R. Weih, L. Rezzolla, and J. Schaffner-Bielich, *Phys. Rev. Lett.* **120**, 261103 (2018).
- [15] Y. Lim and J. W. Holt, *Phys. Rev. Lett.* **121**, 062701 (2018).
- [16] I. Tews, J. Carlson, S. Gandolfi, and S. Reddy, *Astrophys. J.* **860**, 149 (2018).
- [17] Y.-M. Kim, Y. Lim, K. Kwak, C. H. Hyun, and C.-H. Lee, *Phys. Rev. C* **98**, 065805 (2018).
- [18] K. Hebeler and A. Schwenk, *Phys. Rev. C* **82**, 014314 (2010).
- [19] S. Gandolfi, J. Carlson, and S. Reddy, *Phys. Rev. C* **85**, 032801 (2012).
- [20] A. Gezerlis, I. Tews, E. Epelbaum, S. Gandolfi, K. Hebeler, A. Nogga, and A. Schwenk, *Phys. Rev. Lett.* **111**, 032501 (2013).
- [21] A. Carbone, A. Rios, and A. Polls, *Phys. Rev. C* **90**, 054322 (2014).
- [22] G. Hagen, T. Papenbrock, A. Ekström, K. Wendt, G. Baardsen, S. Gandolfi, M. Hjorth-Jensen, and C. Horowitz, *Phys. Rev. C* **89**, 014319 (2014).
- [23] A. Roggero, A. Mukherjee, and F. Pederiva, *Phys. Rev. Lett.* **112**, 221103 (2014).
- [24] G. Wlazłowski, J. W. Holt, S. Moroz, A. Bulgac, and K. J. Roche, *Phys. Rev. Lett.* **113**, 182503 (2014).
- [25] S. Gandolfi, A. Gezerlis, and J. Carlson, *Ann. Rev. Nucl. Part. Sci.* **65**, 303 (2015).
- [26] F. Sammarruca, L. Coraggio, J. W. Holt, N. Itaco, R. Machleidt, and L. E. Marcucci, *Phys. Rev. C* **91**, 054311 (2015).
- [27] C. Drischler, A. Carbone, K. Hebeler, and A. Schwenk, *Phys. Rev. C* **94**, 054307 (2016).
- [28] J. W. Holt and N. Kaiser, *Phys. Rev. C* **95**, 034326 (2017).
- [29] N. K. Glendenning, *Phys. Lett.* **B114**, 392 (1982).
- [30] N. K. Glendenning and S. A. Moszkowski, *Phys. Rev. Lett.* **67**, 2414 (1991).
- [31] S. Weissenborn, D. Chatterjee, and J. Schaffner-Bielich, *Nucl. Phys. A* **881**, 62 (2012).
- [32] S. Weissenborn, D. Chatterjee, and J. Schaffner-Bielich, *Phys. Rev. C* **85**, 065802 (2012).
- [33] Y. Lim, C. H. Hyun, K. Kwak, and C.-H. Lee, *Int. J. Mod. Phys. E* **24**, 1550100 (2015).
- [34] Y. Lim, C.-H. Lee, and Y. Oh, *Phys. Rev. D* **97**, 023010 (2018).
- [35] D. Kaplan and A. Nelson, *Phys. Lett.* **B175**, 57 (1986).
- [36] V. Thorsson, M. Prakash, and J. M. Lattimer, *Nucl. Phys. A* **572**, 693 (1994).
- [37] C.-H. Lee, *Phys. Rept.* **275**, 255 (1996).
- [38] N. K. Glendenning and J. Schaffner-Bielich, *Phys. Rev. Lett.* **81**, 4564 (1998).
- [39] Y. Lim, K. Kwak, C. H. Hyun, and C.-H. Lee, *Phys. Rev. C* **89**, 055804 (2014).
- [40] G. Baym, *Phys. Rev. Lett.* **30**, 1340 (1973).
- [41] C.-K. Au and G. Baym, *Nucl. Phys. A* **236**, 500 (1974).
- [42] M. Prakash, J. R. Cooke, and J. M. Lattimer, *Phys. Rev. D* **52**, 661 (1995).
- [43] F. Weber, *Prog. Part. Nucl. Phys.* **54**, 193 (2005).
- [44] S. Weissenborn, I. Sagert, G. Pagliara, M. Hempel, and J. Schaffner-Bielich, *Astrophys. J.* **740**, L14 (2011).
- [45] H. Liu, J. Xu, and C. M. Ko, [arXiv:1908.01918](https://arxiv.org/abs/1908.01918) (2019).
- [46] D. Pines and M. A. Alpar, *Nature (London)* **316**, 27 (1985).
- [47] B. Link, R. I. Epstein, and J. M. Lattimer, *Phys. Rev. Lett.* **83**, 3362 (1999).
- [48] N. Andersson, K. Glampedakis, W. C. G. Ho, and C. M. Espinoza, *Phys. Rev. Lett.* **109**, 241103 (2012).
- [49] Chamel, N., Fantina, A. F., Pearson, J. M., and Goriely, S., *Astron. Astrophys.* **553**, A22 (2013).
- [50] W. C. G. Ho, C. M. Espinoza, D. Antonopoulou, and N. Andersson, *Sci. Adv.* **1** (2015).
- [51] G. Watanabe and C. J. Pethick, *Phys. Rev. Lett.* **119**, 062701 (2017).
- [52] T. Güver, F. Özel, A. Cabrera-Lavers, and P. Wroblewski, *Astrophys. J.* **712**, 964 (2010).
- [53] S. Guillot and R. E. Rutledge, *Astrophys. J. Lett.* **796**, L3 (2014).
- [54] F. Özel and P. Freire, *Ann. Rev. Astron. Astrophys.* **54**, 401 (2016).
- [55] A. W. Steiner, J. M. Lattimer, and E. F. Brown, *Eur. Phys. J. A* **52**, 18 (2016).
- [56] V. F. Suleimanov, J. Poutanen, J. Nttil, J. J. E. Kajava, M. G. Revnirtsev, and K. Werner, *Mon. Not. Roy. Astr. Soc.* **466**, 906 (2016).
- [57] Nättilä, J., Miller, M. C., Steiner, A. W., Kajava, J. J. E., Suleimanov, V. F., and Poutanen, J., *Astron. Astrophys.* **608**, A31 (2017).
- [58] D. Page, *Astrophys. J.* **428**, 250 (1994).
- [59] D. Yakovlev and C. Pethick, *Ann. Rev. Astron. Astrophys.* **42**, 169 (2004).
- [60] D. Page, J. M. Lattimer, M. Prakash, and A. W. Steiner, *Astrophys. J. Suppl.* **155**, 623 (2004).
- [61] D. Page, J. M. Lattimer, M. Prakash, and A. W. Steiner, *Astrophys. J.* **707**, 1131 (2009).
- [62] C. O. Heinke and W. C. G. Ho, *Astrophys. J. Lett.* **719**, L167 (2010).
- [63] D. Page, M. Prakash, J. M. Lattimer, and A. W. Steiner, *Phys. Rev. Lett.* **106**, 081101 (2011).
- [64] Y. Lim, C. H. Hyun, and C.-H. Lee, *Int. J. Mod. Phys. E* **26**, 1750015 (2017).
- [65] Y. Lim, C. H. Hyun, and C.-H. Lee, (2016), [arXiv:1608.02078 \[nucl-th\]](https://arxiv.org/abs/1608.02078).
- [66] E. F. Brown, A. Cumming, F. J. Fattoyev, C. J. Horowitz, D. Page, and S. Reddy, *Phys. Rev. Lett.* **120**, 182701 (2018).
- [67] I. A. Morrison, T. W. Baumgarte, S. L. Shapiro, and V. R. Pandharipande, *Astrophys. J.* **617**, L135 (2004).
- [68] M. Bejger, T. Bulik, and P. Haensel, *Mon. Not. R. Astron. Soc.* **364**, 635 (2005).
- [69] Y. Lim, J. W. Holt, and R. J. Stahulak, *Phys. Rev. C* **100**, 035802 (2019).
- [70] S. Bogdanov *et al.*, [arXiv:1903.04648](https://arxiv.org/abs/1903.04648) (2019).
- [71] D. Psaltis, F. Özel, and D. Chakrabarty, *Astrophys. J.* **787**, 136 (2014).
- [72] F. Özel, D. Psaltis, Z. Arzoumanian, S. Morsink, and M. Baubck, *Astrophys. J.* **832**, 92 (2016).
- [73] J. S. Read, B. D. Lackey, B. J. Owen, and J. L. Friedman, *Phys. Rev. D* **79**, 124032 (2009).
- [74] K. Hebeler, J. M. Lattimer, C. J. Pethick, and A. Schwenk, *Phys. Rev. Lett.* **105**, 161102 (2010).
- [75] C. A. Raithel, F. Özel, and D. Psaltis, *Astrophys. J.* **831**, 44 (2016).
- [76] L. Lindblom, *Phys. Rev. D* **82**, 103011 (2010).
- [77] F. J. Fattoyev, W. G. Newton, and B.-A. Li, *Eur. Phys. J. A* **50**, 45 (2014).
- [78] J. Margueron, R. Hoffmann Casali, and F. Gulminelli,

- Phys. Rev. C **97**, 025806 (2018).
- [79] P. Bedaque and A. W. Steiner, Phys. Rev. Lett. **114**, 031103 (2015).
- [80] H. T. Janka and E. Mueller, Astron. Astrophys. **306**, 167 (1996).
- [81] M. Rampp and H. T. Janka, Astron. Astrophys. **396**, 361 (2002).
- [82] K. Kifonidis, T. Plewa, H. T. Janka, and E. Mueller, Astron. Astrophys. **408**, 621 (2003).
- [83] R. Buras, M. Rampp, H. T. Janka, and K. Kifonidis, Astron. Astrophys. **447**, 1049 (2006).
- [84] K. Kotake, K. Sato, and K. Takahashi, Rept. Prog. Phys. **69**, 971 (2006).
- [85] H.-T. Janka, K. Langanke, A. Marek, G. Martinez-Pinedo, and B. Mueller, Phys. Rept. **442**, 38 (2007).
- [86] C. D. Ott, Class. Quan. Grav. **26**, 063001 (2009).
- [87] J. W. Murphy, C. D. Ott, and A. Burrows, Astrophys. J. **707**, 1173 (2009).
- [88] L. F. Roberts, C. D. Ott, R. Haas, E. P. O'Connor, P. Diener, and E. Schnetter, Astrophys. J. **831**, 98 (2016).
- [89] M. Ruffert and H. T. Janka, Astron. Astrophys. **338**, 535 (1998).
- [90] M. Ruffert and H. T. Janka, Astron. Astrophys. **344**, 573 (1999).
- [91] M. Ruffert, H. T. Ruffert, and H. T. Janka, Astron. Astrophys. **380**, 544 (2001).
- [92] Oechslin, R., Janka, H.-T., and Marek, A., Astron. Astrophys. **467**, 395 (2007).
- [93] A. Bauswein, H.-T. Janka, and R. Oechslin, Phys. Rev. D **82**, 084043 (2010).
- [94] A. Bauswein, H.-T. Janka, K. Hebeler, and A. Schwenk, Phys. Rev. D **86**, 063001 (2012).
- [95] O. Korobkin, S. Rosswog, A. Arcones, and C. Winteler, Mon. Not. Roy. Astron. Soc. **426**, 1940 (2012).
- [96] M. Tanaka and K. Hotokezaka, Astrophys. J. **775**, 113 (2013).
- [97] D. Kasen, B. Metzger, J. Barnes, E. Quataert, and E. Ramirez-Ruiz, Nature **551**, 80 EP (2017).
- [98] F.-K. Thielemann, M. Eichler, I. Panov, and B. Wehmeyer, Ann. Rev. Nucl. Part. Sci. **67**, 253 (2017).
- [99] J. M. Lattimer and D. N. Schramm, Astrophys. J. **192**, L145 (1974).
- [100] J. M. Lattimer and D. N. Schramm, Astrophys. J. **210**, 549 (1976).
- [101] D. Radice, A. Perego, K. Hotokezaka, S. A. Fromm, S. Bernuzzi, and L. F. Roberts, Astrophys. J. **869**, 130 (2018).
- [102] J. Lattimer, C. Pethick, D. Ravenhall, and D. Lamb, Nucl. Phys. A **432**, 646 (1985).
- [103] J. M. Lattimer and F. D. Swesty, Nucl. Phys. A **535**, 331 (1991).
- [104] Y. Lim, *Theory of nuclear matter of neutron stars and core collapsing supernovae*, Ph.D. thesis, Stony Brook University (2012).
- [105] A. S. Schneider, L. F. Roberts, and C. D. Ott, Phys. Rev. C **96**, 065802 (2017).
- [106] H. Shen, H. Toki, K. Oyamatsu, and K. Sumiyoshi, Nucl. Phys. A **637**, 435 (1998).
- [107] G. Shen, C. J. Horowitz, and S. Teige, Phys. Rev. C **83**, 035802 (2011).
- [108] H. Shen, H. Toki, K. Oyamatsu, and K. Sumiyoshi, Astrophys. J. Suppl. **197**, 20 (2011).
- [109] M. Hempel and J. Schaffner-Bielich, Nucl. Phys. A **837**, 210 (2010).
- [110] M. Hempel, T. Fischer, J. Schaffner-Bielich, and M. Liebendrfel, Astrophys. J. **748**, 70 (2012).
- [111] S. Furusawa, S. Yamada, K. Sumiyoshi, and H. Suzuki, Astrophys. J. **738**, 178 (2011).
- [112] L. Baiotti, B. Giacomazzo, and L. Rezzolla, Phys. Rev. D **78**, 084033 (2008).
- [113] C. Wellenhofer, J. W. Holt, N. Kaiser, and W. Weise, Phys. Rev. C **89**, 064009 (2014).
- [114] C. Wellenhofer, J. W. Holt, and N. Kaiser, Phys. Rev. C **92**, 015801 (2015).
- [115] A. Carbone and A. Schwenk, Phys. Rev. **C100**, 025805 (2019).
- [116] J.-J. Lu, Z.-H. Li, G. F. Burgio, and H. J. Schulze, arXiv:1907.03120 (2019).
- [117] C. A. Raithel, F. Ozel, and D. Psaltis, Astrophys. J. **875**, 12 (2019).
- [118] P. Navrátil, V. G. Gueorguiev, J. P. Vary, W. E. Ormand, and A. Nogga, Phys. Rev. Lett. **99**, 042501 (2007).
- [119] E. Epelbaum, H. Krebs, T. A. Lähde, D. Lee, U.-G. Meißner, and G. Rupak, Phys. Rev. Lett. **112**, 102501 (2014).
- [120] K. Hebeler, J. D. Holt, J. Menendez, and A. Schwenk, Ann. Rev. Nucl. Part. Sci. **65**, 457 (2015).
- [121] J. W. Holt, M. Rho, and W. Weise, Phys. Rept. **621**, 2 (2016).
- [122] A. Carbone, A. Polls, and A. Rios, Phys. Rev. C **98**, 025804 (2018).
- [123] X. Du, A. W. Steiner, and J. W. Holt, Phys. Rev. C **99**, 025803 (2019).
- [124] N. Chamel, S. Goriely, and J. M. Pearson, Phys. Rev. C **80**, 065804 (2009).
- [125] P. Donati, P. M. Pizzochero, P. F. Bortignon, and R. A. Broglia, Phys. Rev. Lett. **72**, 2835 (1994).
- [126] G. E. Brown, J. H. Gunn, and P. Gould, Nucl. Phys. **46**, 598 (1963).
- [127] G. F. Bertsch and T. T. S. Kuo, Nucl. Phys. **A112**, 204 (1968).
- [128] E. Rrapaj, A. Roggero, and J. W. Holt, Phys. Rev. C **93**, 065801 (2016).
- [129] C. Constantinou and M. Prakash, Phys. Rev. **C95**, 055802 (2017).
- [130] B.-A. Li, B.-J. Cai, L.-W. Chen, and J. Xu, Prog. Part. Nucl. Phys. **99**, 29 (2018).
- [131] N. Ismail, M. Buraczynski, and A. Gezerlis, Phys. Rev. Lett. **122**, 152701 (2019).
- [132] J. W. Holt, N. Kaiser, and W. Weise, Nucl. Phys. **A876**, 61 (2012).
- [133] P. B. Demorest, T. Pennucci, S. M. Ransom, M. S. E. Roberts, and J. W. T. Hessels, Nature **467**, 1081 (2010).
- [134] J. Antoniadis *et al.*, Science **340**, 6131 (2013).
- [135] Y. Lim and J. W. Holt, Phys. Rev. C **95**, 065805 (2017).
- [136] G. Baym, H. A. Bethe, and C. J. Pethick, Nucl. Phys. A **175**, 225 (1971).
- [137] G. Baym, C. Pethick, and P. Sutherland, Astrophys. J. **170**, 299 (1971).
- [138] N. Chamel and P. Haensel, Living Rev. Rel. **11** (2008).
- [139] K. Hebeler, J. M. Lattimer, C. J. Pethick, and A. Schwenk, Astrophys. J. **773**, 11 (2013).
- [140] H.-T. Janka, T. Zwerger, and R. Moenchmeyer, Astron. Astrophys. **268**, 360 (1993).
- [141] H. Yasin, S. Schfer, A. Arcones, and A. Schwenk,

- (2018), arXiv:1812.02002 [nucl-th] .
- [142] C. Constantinou, B. Muccioli, M. Prakash, and J. M. Lattimer, Phys. Rev. **C92**, 025801 (2015).
- [143] J. M. Lattimer and Y. Lim, Astrophys. J. **771**, 51 (2013).
- [144] J. W. Holt and Y. Lim, Phys. Lett. **B784**, 77 (2018).
- [145] C. Wellenhofer, J. W. Holt, and N. Kaiser, Phys. Rev. C **93**, 055802 (2016).
- [146] Y. Lim and J. W. Holt, “Nuclear equation of state for hot dense matter constrained by chiral effective field theory,” In preparation.